Chapter 4

Chapter 4. Tracing the anti-cancer mechanism of HFPO1 by the integrative approach of network pharmacology and experimental studies

4.1. Background

In the previous chapter, hexane fraction of DCM: Et crude extract of *P. osteratus* (HFPO1) excels in cytotoxic potential against panels of the cancer cell lines, owing to the presence of a high abundance of cholestane steroids, terpenoid (sesterterpenoid, diterpenoid, sesquiterpenoid, and triterpenoid), fatty alcohol, and steroidal alkaloid class of myco-metabolites. The present chapter tries to explore the mechanistic pathway of HFPO1 against breast, blood, and lung cancer *via* network pharmacology along with experimental validation. Initially, myco-metabolites tentatively identified were screened based on drug-likeness properties, targets of the myco-metabolites, and diseases (breast, blood, and lung cancer) were predicted from the online web server, and overlapping targets were further selected. Influential hub targets were identified by network analysis of protein-protein interaction (PPI). Further, Gene enrichment analysis of these target genes was performed *via* gene ontology (GO) and Kyoto Encyclopaedia of Genes and Genomes (KEGG). Molecular docking of the hub target with their selected myco-metabolites was studied. Predicted target genes involved in the KEGG pathway of cancer were further validated by immunoblot analysis of target protein expression of HFPO1 treated cell line, along with anti-tumor activity against Ehrlich ascites carcinoma (EAC) in Swiss albino mice.

4.2. Objectives

- Elucidation of mechanistic pathways of myco-metabolites of HFPO1 against cancer using network pharmacology.
- Elucidation of mechanistic pathways of myco-metabolites of HFPO1 against cancer using experimental methods.
    - *In-vitro* fluorescence imaging and immunoblot analysis of HFPO1 treated cancer cell line.
    - *In-vivo* anti-tumor activity of HFPO1 treated EAC (solid tumor) bearing Swiss albino mice, along with acute toxicity profile of HFPO1 in Swiss albino mice.

4.3. Experimental work

4.3.1. Preliminary work

Preliminary results on HFPO1 showed promising cytotoxicity against human blood, breast, and lung cancer cell lines (IC_{50} < 200 µg/mL), and LC-QTOF/MS untargeted myco-metabolite screening tentatively identified twelve myco-metabolites. These twelve myco-metabolites were: betulin (BET), solanocapsine (SOL), asterosterol (AST), (3b,6b,8a,12a)-8,12-epoxy-7(11)-eremophilene-6,8,12-trimethoxy-3-ol (ERE), beta-obscurine (OBS), myxalamid B (MYX), momordol (MOM), avocadyne 4-acetate (AVO), ophiobolin F (OPH), linoleoyl ethanolamide (LIN), (13R,14R)-7-Labdene-13,14,15-triol (LAB), and cholest-5-ene (CHOL).

4.3.2. Network pharmacology

4.3.2.1. *In-silico* drug-likeness screening

Oral bioavailability is the key determinant for a molecule to be biologically and physiologically active. The drug-likeness screening was assessed based on Lipinski's rule of five. *In-silico* oral bioavailability and drug-likeness were determined by an online web server Swiss ADME (http://www.swissadme.ch/, accessed on 26 November 2021) (Daina et al., 2017). The myco-metabolites with oral bioavailability score > 0.5, following Lipinski's rule of five, were screened out for further analysis.

4.3.2.2. Compound-target prediction

The SMILES (Simplified Molecular Input Line Entry System) of identified myco-metabolites were retrieved from the PubChem database. Swiss target prediction, an online target prediction web server (http://www.swisstargetprediction.ch/, accessed on 28 November 2021) was used for the target prediction of identified myco-metabolites. From the 'n' numbers of target prediction, targets with a green bar were identified for further exploration. The green bar is indicative of the probability of protein to be a target for query molecule, value ≤ 1. A higher value (more the length of the green bar) reflects a higher probability of protein being a target for the query molecule (Daina et al., 2019).

4.3.2.3. Diseases-target prediction

Information related to target genes associated with the diseases: blood cancer, breast cancer, and lung cancer were obtained from MalaCards (https://www.malacards.org/#, accessed on 3rd December 2021) and DisGeNet (https://www.disgenet.org/search, accessed on 16th December 2021) with three different keywords: Hematologic cancer, breast cancer, and lung cancer. MalaCards is an integrated database on human maladies and their annotation along with their associated target genes (in association with GeneCard). It encompasses numerous aliases for each disease under one umbrella

(Rappaport et al., 2017). Whereas, DisGeNet integrated information on human gene-disease associations (GDAs) and variant-disease associations (VDAs) (Piñero et al., 2017).

The target genes of the myco-metabolites from Swiss target prediction were compared with the target genes of the disease from MalaCards and DisGeNet individually, and the matched target genes were selected. These matched target genes from both database were again compared, and overlapping target genes were screened for analysis.

4.3.2.4. Protein-protein interaction

To predict physical and functional interaction between the overlapping target genes and to understand the mechanistic approach, the protein-protein interaction was constructed by Search Tool for the Retrieval of Interacting Genes/ Protein (STRING) (https://string-db.org/, accessed on 28th January 2022) under the setting of confidence level between the protein-protein interaction as high as 0.9 (Szklarczyk et al., 2015). Nodes (protein) with no edges (interaction) were excluded, and the resultant protein-protein interaction network was further launched into the Cytoscape tool (Cytoscape; Version 3.8.2.) for evaluation of topological features of the network (Shannon et al., 1971).

4.3.2.5. Gene enrichment analysis

GO, and KEGG pathway of the resultant protein associated with protein-protein interaction (STRING) was analyzed by ShinyGO (http://bioinformatics.sdstate.edu/go/, accessed on 30th January 2022) (Ge et al., 2020). GO is mainly carried out to analyze and describe genomic information in terms of associated biological processes, cellular components, and molecular functions. The KEGG pathway is used to retrieve information regarding gene function annotation and its involvement in the underlying

metabolic pathway of target-associated disease. Both the analysis diminishes the redundancy of results and thus, improvises the data prediction.

4.3.2.6. Network layout of compound-target

Graphical visualization of a network between myco-metabolites with target genes enriched in strong protein-protein interaction was constructed using the Cytoscape tool (Cytoscape; Version 3.8.2.), and network analysis were executed (Shannon et al., 1971).

4.3.2.7. *In-silico* molecular docking

The molecular docking studies use the automated docking program AutoDock4.2 based on a genetic algorithm(Morris et al., 2009). The study was carried out in three steps: (a) Protein preparation, (b) Ligands preparation, and (c) Simulation of automated docking for studying the *in-silico* docking interaction of hub targets with their key myco-metabolites.

(a) Protein preparation: The protein data bank (https://www.rcsb.org/, accessed on 4th March 2022) was used to get the X-ray crystal structures of hub targets PIK3CA, MAPK3, AKT1, JAK2, ESR1, and EGFR (Morris et al., 2009). The study was conducted on only a single subunit of the protein dimer. Using Discovery Studio 2019 Client, the additional chains comprising heteroatoms, co-crystallized ligands, and water molecules were eliminated. These final edited structures of enzymes were saved as a PDB file, which was further used for the final docking with test and reference compounds.

(b) Ligand Preparation: 2D structures of all the selective compounds against specific targets were drawn in ChemDraw Professional 15.0 and saved in PDB format by Chem3D 15.0 with minimized energy by the MM2 force field and were used for final docking.

(c) Simulation of automated docking: The protein file was loaded on AutoDock Tools (ADT; version 1.5.4). The missing hydrogen atoms were added. Non-polar hydrogens were combined, and protein charges were added using Gasteiger–Marsili charges and Kollman charges. Further, the ligand PDB files were loaded into the AutoDock 4.2 program, flexible torsions were assigned using the Autodock module, and the acyclic dihedral angles were allowed to rotate freely. After that, the file was converted to pdbqt format. After preparing both pdbqt files, we generated the grid box that defines the specific site of binding of the ligand in protein. The output of the grid was saved in gpf (grid parameter file). We also prepared the dpf (docking file of ligands. After that, AutoGrid and AutoDock module was run in command prompt, which gave the conformer log dlg file. Further, the docked conformers were analyzed by Discovery Studio 2019 Client.

4.3.2.8. *In-silico* cancer multi-omics expression study & prognostic potential

Before *in-vitro* experimental validation, the mRNA and prognostic potential of selected hub targets (PI3KCA, and AKT1) for acute myeloid leukemia were analysed. The Gene expression profile interactive analysis (GEPIA2) webserver was used for the mRNA expression analysis of the PI3KCA, and AKT1 hub targets for acute myeloid leukaemia (**http://gepia2.cancer-pku.cn/#analysis**, accessed on 2th February 2022) (Tang et al., 2019). GEPIA2, an updated version of GEPIA, analyse RNA sequencing expression of 8587 normal and 9736 tumor samples from The Cancer Genome Atlas (TCGA) and Genotype-Tissue Expression dataset (GTEx). For establishing the role of PI3KCA, and AKT1 hub targets in the survival of patients with acute myeloid leukaemia, UALCAN webserver (**http://ualcan.path.uab.edu/cgi-bin/ualcan-res.pl**, accessed on 4th February 2022) was used (Chandrashekar et al., 2017). The median expression of genes served as

the cut-off value for classifying patients into high and low-expression groups, for the overall survival analysis of PI3KCA, and AKT1 in acute myeloid leukemia patients.

4.3.3. *In-vitro* experimental validation

4.3.3.1. Fluorescence microscopy

HL-60 cells were treated with 0, 50, 100, and 200 µg/mL concentrations of HFPO1 for 48 hours. After the treatment, treated cells were collected, washed with PBS twice, fixed in 400 µL cold acetic acid and methanol (1:3, v/v), and left overnight at 4˚C. The next day, cells were washed, dispensed in 50 µL of fixing solution, spread on a clean slide, and dried overnight at room temperature. Further cells were stained with DAPI (5 µg/mL DAPI in 0.01M citric acid and 0.45M disodium phosphate containing 0.05% Tween 20) for 30 min at room temperature, and subsequently, the slides were washed with distilled water, followed by PBS washing. While in wet condition, 40 µL of mounting fluid (PBS: Glycerol, 1:1 v/v) was poured over the slide and covered with a glass coverslip. Cells were observed under a microscope for any nuclear morphological changes, such as chromatin condensation and nuclear shrinkage as indicative of apoptosis. For phase-contrast microscopy, cells were simply photographed using a microscope after the treatment (Guru et al., 2015).

4.3.3.2. Immunoblot analysis

Approximately 2×10^6 HL-60 cells/well were seeded and treated with different concentrations of HFPO1 (0, 50, 100, and 200 µg/mL) for 48 hours. After 48 hours of treatment, the cells were harvested with trypsin and centrifuged at 1400 RPM for 5 min. After centrifugation, the supernatant was aspirated, and pellets were washed with cold PBS (around 4˚C). Further, pellets were resuspended in an appropriate volume of cold RIPA lysis buffer, freshly supplemented with 1% (v/v) eukaryotic protease inhibitor for 45 min, and vortexed at 10 min intervals while maintaining on ice. Later, centrifuged at

14,000 RPM at 4 ˚C for 15 min, and the resultant supernatant was used as a whole-cell lysate for a protein expression study (Guru et al., 2015).

4.3.4. *In-vivo* experimentation

4.3.4.1. Experimental animals

Prior to the experiment, Institutional Animal Ethics Committee approval (Protocol no. Dean/2021/IAEC/2553) was granted, attached in *Appendix* (Figure A5). Nulliparous female Swiss albino mice (20-25 g) were acquired from the Central animal house, Institute of Medical Sciences, Banaras Hindu University (BHU), Varanasi, India. Animals were housed under standard laboratory conditions such as a temperature of 21 ± 2˚C, relative humidity of 55 ± 5%, a 12-hour light-dark cycle, and freely accessible food and water. Before commencing the experiment, the animals were acclimatized for two weeks. All the experiments were in accordance with the Committee for the Purpose of Control and Supervision of Experiments on Animals (CPCSEA), Government of India, New Delhi.

4.3.4.2. Acute toxicity assessment

Acute toxicity assay was conducted in accordance with the Organisation for Economic Co-operation and Development (OECD) Guidelines for the Testing of Chemicals, Acute oral toxicity: Up-Down Procedure, Test No. 425. Owing to a lack of information on the toxicity profile of the substance, the main test was conducted with starting default dose of 175 mg/kg p.o. (in 0.5%w/v carboxymethylcellulose (CMC)) as a single dose. Prior to dosing, mice were kept on fasting (without food for 3-4 h but had access to water) and weighed. After the administration of substances, food was withheld for 1-2 hours, and the animal was observed for 48 hours. The short-term outcome (for 48 hours) of the administrated dose was reported as death or survival; this data was fed in AOT425STATPgm software. AOT425STATPgm software (developed by Westat for the

US EPA), a user interface, was used to facilitate animal-by-animal calculation that establishes testing sequences and provides the final estimation of LD_{50}, by using the maximum likelihood method (OECD, 2002). The resultant surviving mice were observed for 14 days, and at the end of the 14th day, they were weighed, and blood was collected by cardiac puncture under anesthesia with isoflurane for biochemical and hematological estimation. The kidney and liver of humanely killed mice were excised and preserved in 10% formalin for histopathological evaluation.

4.3.5. *In-vivo* anti-tumor efficacy in EAC (solid tumor) bearing Swiss albino mice

EAC cell lines were inoculated into the peritoneal cavity of female Swiss albino mice to propagate. After 7-8 days, ascetic fluid containing EAC cells was collected, examined for cell viability, and counted by a hemocytometer. Accurately, 2.5×10^6 EAC cells were injected subcutaneously into a mammary pad for the development of a solid tumor (Saneja et al., 2017). After 4-5 days, mice bearing approximately 45 mm^3 tumor volume were scrutinized and randomized into 5 groups (5 animal/group) as follows. Group I: tumor-bearing mice (T); Groups II, III, and IV: tumor-bearing mice treated with a dose of 5 mg/kg p.o. (H1), 10 mg/kg p.o. (H2) and 15 mg/kg p.o. (H3) of HFPO1, respectively for three alternate days for a period of 15 days; and Group V: tumor-bearing mice received the standard drug paclitaxel 10 mg/kg p.o. (S), for three alternate days. The control group receiving 0.5%w/v CMC (N) was also included in this study as Group VI. On the 0th and 15th days, tumor volume and body weight were recorded. Tumor volume was measured by vernier caplier using the following equation 4.1.

$$Tumor\ volume = \frac{l\times w^2}{2} \qquad \textbf{Equation 4.1.}$$

Where, l represents the largest tumor diameter, and w represents the perpendicular tumor diameter. At the end of the study, animals were humanely killed, and tumor weight was

recorded. Methodology for *in-vivo* anti-tumor efficacy of HFPO1 in EAC (solid tumor) bearing Swiss albino mice is schematically described in Figure 4.1.

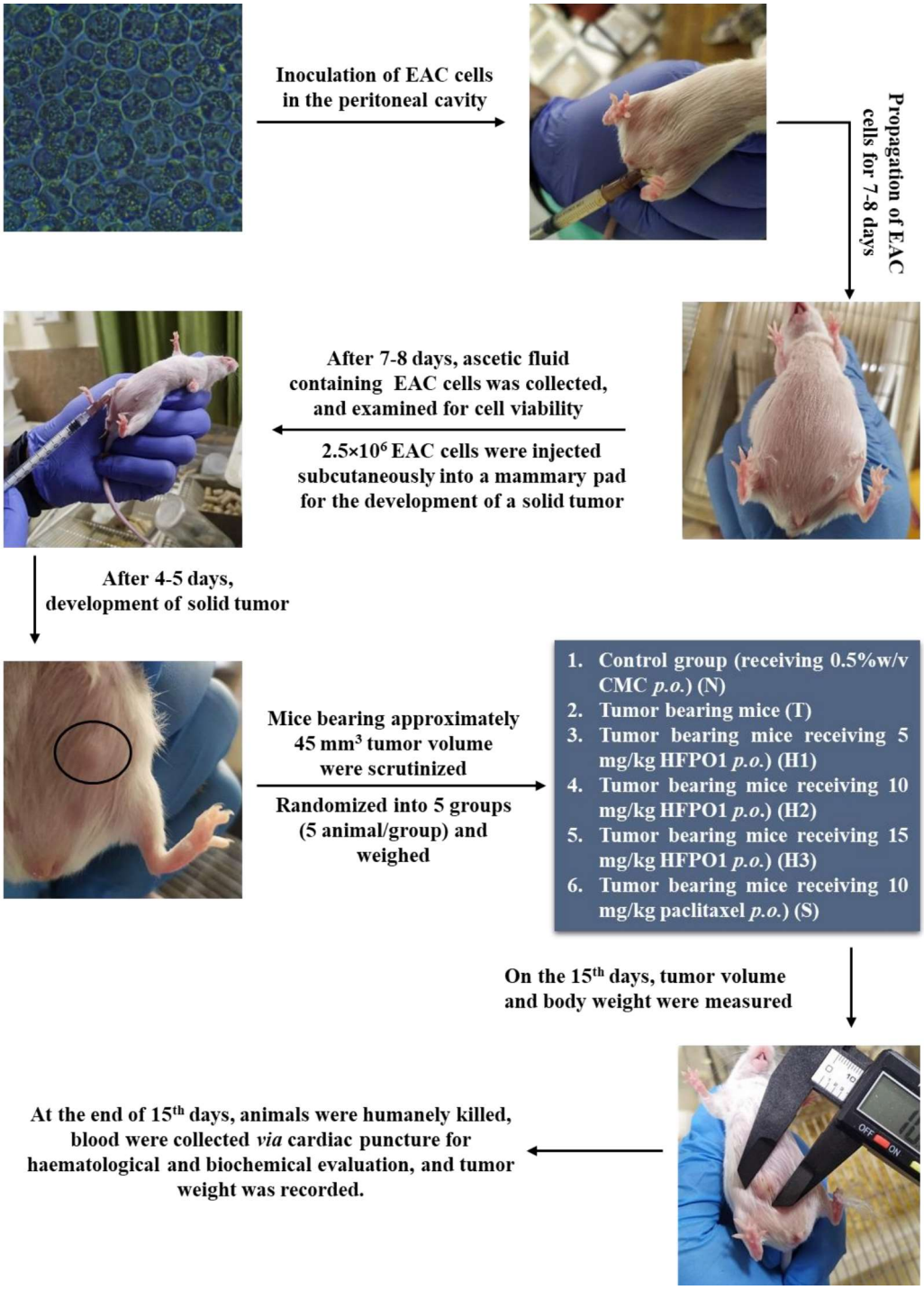

Figure 4.1. Methodology for *in-vivo* anti-tumor efficacy of HFPO1 in EAC (solid tumor) bearing Swiss albino mice**.**

4.4. Results and Discussion

4.4.1. Network pharmacology

4.4.1.1. *In-silico* drug-likeness screening

The myco-metabolites tentatively identified were evaluated based on the drug-likeness properties following Lipinski's rule of 5. Remarkably, all the tentatively identified molecules (12) pass Lipinski's rule of 5 with a bioavailability score > 0.5, as shown in Table 4.1. Four compounds (BET, OPH, AST, and CHOL) violated one of the rules of Lipinski with MLogP greater than 5, hence overruled.

Table 4.1. Drug-likeness properties of tentatively identified myco-metabolites.

Molecule	MW	HBA	HBD	MlogP	Lipinski violations	Bioavailability Score
BET	442.72	2	2	6	1	0.55
SOL	430.67	4	3	4.23	1	0.55
OPH	358.6	1	1	5.83	1	0.55
LIN	323.51	2	2	3.64	0	0.55
LAB	324.5	3	3	3.05	0	0.55
AST	370.61	1	1	6.03	1	0.55
CHOL	370.65	0	0	8.32	1	0.55
ERE	326.43	5	1	1.32	0	0.55
OBS	272.39	2	1	2.87	0	0.55
MYX	401.58	3	3	3.53	0	0.55
MOM	440.66	5	4	2.54	0	0.55
AVO	326.47	4	2	3.07	0	0.55

MW: Molecular weight; HBA: Hydrogen bond acceptor; HBD: Hydrogen bond donor

4.4.1.2. Compound-target prediction

From 12 tentatively identified myco-metabolites, 10 myco-metabolites were assigned predicted targets. Whereas for ERE and MYX, no similar actives were found; hence no targets were predicted. Uniprot accession ID and the gene symbol of the predicted target were preserved for further exploration. The list of the predicted target for the individual compound is shown in Table 4.2.

Table 4.2. List of the predicted targets for tentatively identified myco-metabolites.

BET	SOL	OPH	LIN	LAB	AST	OBS	CHOL	MOM	AVO
P28845	P04062	P11511	P21554	P10275	P10275	P22303	P22303	P11511	P17252
P16662	O43451	P10275	Q8NER1	P11511	P23975	P35372	P03372	P56817	P48048
Q13133	P14410	Q92731	P34972	P04278	P11511	P41143	P33261	P28845	P06213
P23219	Q9HCG7	P03372	Q07869	P22303	P22303	Q99720	Q07869	P49354 P49356	P00742
P06276	O15244	P18031	Q8TDV5	P06276	P33261	P14416	P34972	P09917	Q08881
P11511	Q96FL8	P33261	O00519	P08172	Q13133	P31213	P11511	P24723	
P18031	P10253	P31645	P34913	P33261	P05093	P35462	P08172	P31213	
Q9UBE0 Q9UBT2	P35573	P05093	P80365	P04035	P06276	O60678	P10275	P01375	
P06746	P32246	Q12772	P06493	P03372	Q9UHC9	P41145	Q05940	P10275	
O60218	P03951	P04035	P37288	P31645	P03372	P36544	P43681 P17787	P35228	
P10275	P23786	P04278	Q9UHC9	P23975	P18031	P43681 P17787	P18031	P0DMS8	
P33261	Q92523	P08172	P48039	Q92731	P04035	Q969F8	Q99720	P18031	
Q9UHC9	P50416	P23975	P49286	P05093	Q16850		Q14994	Q15722	
P34972	Q9GZN0	Q14534	P05067	P18031	P51449		P51449	P04150	
P05093	P11940	Q16850	P28845	Q12772	P31645		Q12772	Q06124	
Q14994	Q5R387	P22303	P20701 P05362 P05107	Q9UHC9	Q92731		Q9UHC9	P06276	
O14684	P31751	P30305	Q16539	Q16850	P04278		Q92731	P03372	
P08172	P31749	Q07869	P04035	Q13133	P08172		P07339	Q92731	
P21731	P04626	Q03181	P00533	P51449	Q14994		P04278	P27361	
P51449	P08253	Q13133	Q16875	P08185	Q12772		P04035	O60218	
P22303	O14672	Q9UHC9	Q00987	P49810 Q9NZ42 Q92542 Q96BI3 P49768 Q8WW43	O14684		Q16850	Q9UHC9	
	Q14703	P06276	P49841	Q16539	O00748		Q8NER1	Q99720	
	P07333	P30304	P35228	Q14534	P30304		P23975	P06401	
	P10721	Q14994	P51449	O14684	P35398		P31645	P20701	
		P15090	P01375	O00748	Q14534		P18405	Q01959	
		P05413	Q14416	P23458	P30305		P31213	O14684	
		Q01469	P35968	O60674	Q9UBM7		P08185	P17706	
		P07148	Q99500	P28845	P29350		P07148	P80365	
		O14684	P21453	Q14994	P17706		P11940	P35398	
		P35398	P53985	P50747	P11413		P48067	O00748	
		P51449	Q99685	P00918	P28845			P43405	
		P32246	P35354	P00915	P08185			O00519	
		P06746	P49810 Q9NZ42 Q92542 Q96BI3 P49768 Q8WW43	P23280	P80365			P08185	

Table 4.2. Continued

BET	SOL	OPH	LIN	LAB	AST	OBS	CHOL	MOM	AVO
		P08185	P45983	P22748	P55055			P04278	
		P10586	O60307	P48147	P11473			P08235	
		P04054	P06737	P23219	P21554			P42345	
		P24666	P30518	P06737	P23415			P05093	
		O00767	P00734	Q13946	P48147			P00797	
		O60218	P55055	P21728	P06746			P14091	
		P28845	O15151	Q9Y233	P54707			P54760	
		Q9UBS5	O00763	P35398	P35228			P21453	
		P08069	P14416	Q5S007	P15090			Q16875	
		P12931	P07711	P28472 P34903 P18507	P05413			P42338	
		P35968	O00767	P28472 P18507 P14867	Q01469			P42336	
		Q9UM73	P25103	P28472 P18507 P31644	Q03181			P49810 Q9NZ42 Q92542 Q96BI3 P49768 Q8WW43	
		P04150	P50750	P47869 P28472 P18507	P07148			P21554	
		P08235	O14920	P32246	P24723			P04035	
			O15111	P49841	P56817			Q15393	
			P00746	P51681	P0DMS8			Q9NWZ3	
			O00748	P05129	P27361			P06746	
			Q13133	P05771	Q06124			P23458	
			P24385 P11802	O15055	O60218			O60674	
			Q99835	P52333	Q99720			Q15118	
			P31213	P09874	P10586			P04629	
			P29371	P29597	P04054			Q00796	
				Q99572	P24666			Q12809	
				O00311	O00767			Q00987	
				Q05469	P16662			P49840	
				P11309	P34972			P07900	
				P25101	P05129			P08238	
				P14555	Q05655			P30304	
				P33981	P05771			Q15904	
				Q9P1W9	Q02156			O76074	
				P78527	Q04759			P29275	
				O60885	P11388			P31645	
				P25440				P09874	
				Q15059				Q13133	
				P21964				P43119	
				Q02750				Q4U2R8	
				Q86V86				P52333	
				O14757				P32246	

Table 4.2. Continued

BET	SOL	OPH	LIN	LAB	AST	OBS	CHOL	MOM	AVO
				Q96RJ0				O00408	
				P15538				Q07343	
				P48039				P35968	
				P19099				P06493	
				P24723				Q8IXJ6	
				P04150				P53671	
				Q9NWZ3				P0DJD9	
				P05186				P29401	
				P35968				P17252	
				O75116				P45983	
				P24941				P08922	
				Q13464				P07333	
				O60725				P45452	
				P42330				P14780	
				P08246				P08253	
				P04629				Q99558	
				P00533				Q15078	
								Q00535	
				P14416				P24864	
								P24941	
				P35462				P08069	
				Q05655				P06213	
				Q13093				P50613	
								P51946	
				Q02156				P50750	
								O60563	
				Q04759				Q08881	
				P35372				P24941	
				P41143				P37268	
				P41145				P20248	
								P24941	
				Q8NG68				O14965	
				P32297				Q16850	
				P30926					
				Q15078				P11362	
				Q00535					

The pink box represents duplicate target genes.

4.4.1.3. Diseases-target prediction

MalaCards database predicted an aggregate of 1056, 150, and 876 target genes for breast cancer (BC), hematologic cancer (HC), and lung cancer (LC), respectively. Comparably, 63, 5, and 46 target genes for BC, HC, and LC overlapped with the myco-metabolites-target gene, respectively, hence resulting in the procurement of a total of 114 target genes as shown in the Table 4.3. Further, the exclusion of duplicate target genes from 114 target genes yields a total of 74 target genes, as shown in the Venn diagram (Figure 4.2.a).

Table 4.3. Overlapped myco-metabolites-target genes with MalaCards diseases-target genes.

LC	BC	HC
PTGES	PIK3CA	KIT
MMP2	AKT1	CSF1R
ESR2	ESR1	JAK2
ESR1	ERBB2	MTOR
CDC25A	CDK2	PTPN11
PLA2G1B	PGR	
IGF1R	CTSD	
KDR	EGFR	
CDK1	MTOR	
MAPK14	ESR2	
EGFR	CYP17A1	
MDM2	CDK1	
TNF	IGF1R	
MAPK8	ROCK1	
CDK2	CHEK1	
NTRK1	CDC25A	
CDK5	MDM2	
MAPK3	TOP2A	
PRKCA	AURKA	
JAK2	MAPK8	
PTPN11	FGFR1	
AKT2	KDR	
AKT1	AKT2	
ERBB2	MMP9	
KIT	MMP2	

Table 4.3. Continued

LC	BC	HC
SRC	MAPK3	
ALK	ALK	
PTGS2	NTRK1	
CTSL	CSF1R	
CDK4	PRKCA	
CHRNB4	PTGS2	
ROCK1	NOS2	
CHEK1	TNF	
MAP2K1	MAP2K1	
TTK	SHBG	
TOP2A	NR3C1	
PGR	KIT	
MTOR	MAPK14	
PIK3CA	MMP13	
HSP90AA1	CDC25B	
FGFR1	HSP90AA1	
AURKA	PRKCD	
TKT	GSK3B	
ROS1	IKBKB	
MMP13	AKR1C3	
MMP9	EPHB4	
	NR3C2	
	CHUK	
	INSR	
	JAK1	
	PIK3CB	
	JAK2	
	EDNRA	
	FABP4	
	SYK	
	PRKCQ	
	FABP3	
	COMT	
	VDR	
	HMGCR	
	NR1H2	
	ROCK2	
	CA2	

The pink box represents duplicate target genes.

DisGeNet database retrieved a total of 19897, 18183, and 10845 target genes for BC, HC, and LC, respectively. Collectively, 515 target genes consisting of 199, 170, and 155 myco-metabolites-target genes matched with BC, HC, and LC diseases-target genes, as

shown in Table 4.4. After removing duplicate target genes from 515 target genes, 223 target genes were left out, as shown in the Venn diagram (Figure 4.2.b).

Table 4.4. Overlapped myco-metabolites-target genes with DisGeNet diseases-target genes.

BC	LC	HC
P28845	Q13133	P23219
P16662	P23219	P06276
P23219	P06276	P11511
P06276	P11511	P18031
P11511	P18031	P10275
P18031	P06746	P33261
P06746	O60218	P34972
O60218	P10275	P05093
P10275	P33261	Q14994
P33261	P05093	O14684
P34972	Q14994	P51449
P05093	O14684	P22303
Q14994	P51449	P32246
O14684	P22303	P11940
P51449	P32246	P08253
P22303	P11940	P07333
P11940	P08253	Q92731
P08253	P07333	P03372
P07333	Q92731	P04035
Q92731	P03372	P04278
P03372	Q12772	P30305
P31645	P23975	Q07869
Q12772	Q14534	P30304
P04035	P30305	P15090
P04278	Q07869	P05413
P23975	Q03181	P35398
Q14534	P30304	P08185
P30305	P15090	P04054
Q07869	P35398	P24666
Q03181	P04054	O00767
P30304	P24666	P08069
P15090	O00767	P35968
P05413	P08069	P04150
Q01469	P35968	P08235
P35398	P04150	P21554
P10586	Q8NER1	Q8NER1
P04054	P80365	P80365
P24666	P06493	P06493

Table 4.4. Continued

LC	BC	HC
O00767	P48039	P48039
P08069	Q16539	Q16539
P35968	P00533	P00533
P04150	Q16875	Q16875
P08235	Q00987	Q00987
P21554	P49841	P49841
Q8NER1	P35228	P35228
O00519	P01375	P01375
P80365	P21453	P21453
P06493	P45983	P45983
P48039	P55055	P55055
Q16539	P14416	P14416
P00533	P23458	O00748
Q16875	O60674	P23458
Q00987	P05771	O60674
P49841	P52333	P48147
P35228	P09874	P05771
P01375	P24941	P52333
P21453	P04629	P09874
P45983	Q05655	P24723
P55055	P35372	Q9NWZ3
P14416	Q15078	P24941
O00748	Q00535	P04629
P31213	P17706	P35462
P23458	P56817	Q05655
O60674	P0DMS8	Q02156
P48147	P27361	Q04759
P05771	Q06124	P35372
P52333	P43681	P41145
P09874	P06213	Q15078
P24723	P17252	Q00535
P24941	Q9UBT2	P17706
P04629	P21731	P27361
P35462	P31751	Q06124
Q05655	P31749	P43681
Q02156	P04626	P06213
Q04759	P10721	Q08881
P35372	Q9UBS5	P17252
Q15078	P12931	Q9UBT2
Q00535	Q9UM73	P04062
P17706	P34913	O15244
P27361	P37288	P50416
Q06124	P05067	P31751
Q99720	P05362	P31749

Table 4.4. Continued

LC	BC	HC
P43681	P05107	P04626
P06213	Q99500	O14672
Q08881	P53985	Q14703
P17252	Q99685	P10721
Q9UBT2	P35354	P12931
Q9UBE0	O15151	Q9UM73
P21731	P07711	P34913
O43451	O14920	P49286
P03951	O15111	P05067
P23786	Q99835	P20701
P50416	P24385	P05362
P31751	P11802	P05107
P31749	P11362	Q99500
P04626	O14965	P53985
O14672	P20248	P35354
Q14703	P37268	P00734
P10721	P50613	O15151
P12931	P51946	O00763
Q9UM73	P24864	P07711
Q8TDV5	Y74	P25103
P49286	P14780	P50750
P05067	P45452	O14920
P20701	P08922	O15111
P05362	Q8IXJ6	Q99835
P05107	O76074	P11802
Q99500	P08238	P00742
P53985	P07900	P11362
Q99685	Q15118	O14965
P35354	P42336	P20248
P30518	P42338	P50750
P00734	P54760	O60563
O15151	P00797	P50613
P07711	P42345	P51946
P25103	P43405	P24864
P50750	Q01959	Q99558
O14920	P06401	P14780
O15111	Q05940	P45452
Q99835	P07339	P08922
P24385	P36544	Q8IXJ6
P11802	Q969F8	Q07343
P00742	P29350	O76074
P48048	P11413	Q15904
P11362	P11473	P08238
O14965	P23415	P07900

Table 4.4. Continued

LC	BC	HC
P20248	P54707	P49840
P50750	P11388	Q12809
P50613	P32297	Q15118
P51946	P30926	P42336
P24864	P08246	P42338
Q99558	P42330	P54760
P14780	O60725	P00797
P45452	Q13464	P42345
P08922	O14757	P43405
P29401	Q02750	P20701
P53671	P21964	P06401
Q8IXJ6	P25440	Q15722
Q07343	O60885	P09917
O00408	P78527	P07339
P29275	Q9P1W9	P36544
O76074	P33981	P29350
P08238	P14555	P11413
P07900	P25101	P11473
Q12809	P11309	P54707
Q00796	Q99572	P11388
Q15118	O15055	P08246
Q15393	P00918	P42330
P42336	P00915	O60725
P42338	Q13946	Q13464
P54760	P21728	O75116
P00797	Q9Y233	O14757
P42345	Q5S007	Q86V86
P43405	P34903	Q02750
Q01959		P21964
P20701		P25440
P06401		O60885
Q15722		P78527
P09917		Q9P1W9
P07339		P33981
P18405		P25101
Q969F8		P11309
P29350		Q05469
P11413		Q99572
P11473		P29597
P11388		O15055
P08246		P51681
P42330		P00918
Q13464		Q5S007
O75116		

Table 4.4. Continued

LC	BC	HC
P05186		
P15538		
Q96RJ0		
O14757		
Q86V86		
Q02750		
P21964		
Q15059		
P25440		
O60885		
P78527		
Q9P1W9		
P33981		
P14555		
P25101		
P11309		
Q05469		
O00311		
Q99572		
P29597		
O15055		
P51681		
P50747		
P00918		
P00915		
P21728		
Q5S007		
P34903		

The pink box represents duplicate target genes.

Finally, 74 target genes from MalaCards and 223 target genes from DisGeNet were matched, resulting in the overlapping of 74 target genes from both the database, as shown in the Venn diagram (Figure 4.2.c). These overlapped 74 target genes may be regarded as the most influential target for BC, HC, and LC.

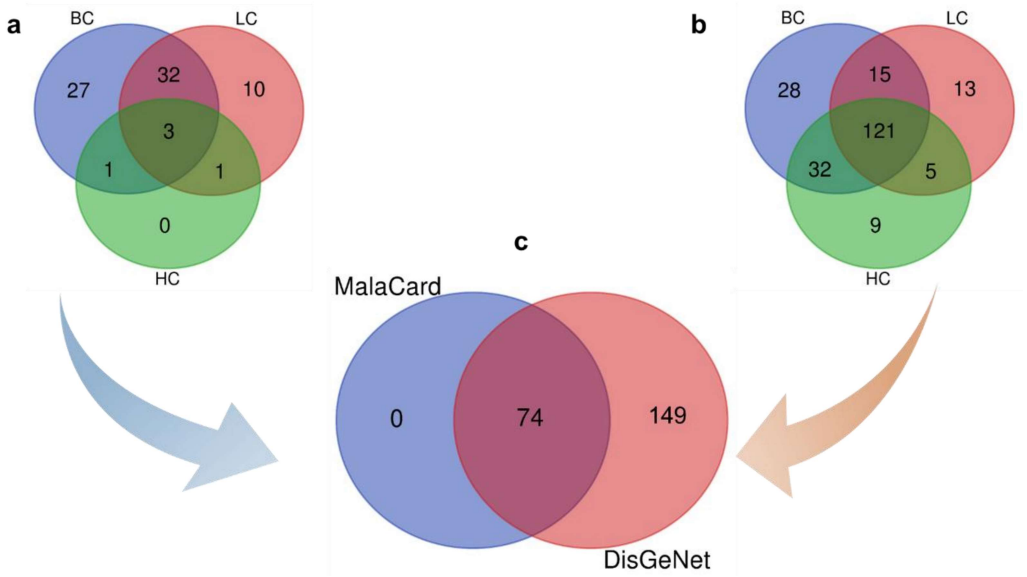

Figure 4.2. Venn diagram of overlapping myco-metabolites-target genes (a) with Malacards database for BC, HC, and LC (b) with DisGeNet database for BC, HC and LC, and (c) altogether from MalaCards and DisGeNet database.

4.4.1.4. Protein-protein interaction

The STRING protein-protein interaction of 74 target genes is shown in Figure 4.3. The interacted STRING protein-protein network has 74 nodes (proteins) connected by 241 edges (interaction) with a local clustering coefficient of 0.448 and an average node degree of 6.51. The p-value (PPI enrichment) was found to be less than 1, thus suggesting that the resultant network has significantly more interaction than excepted.

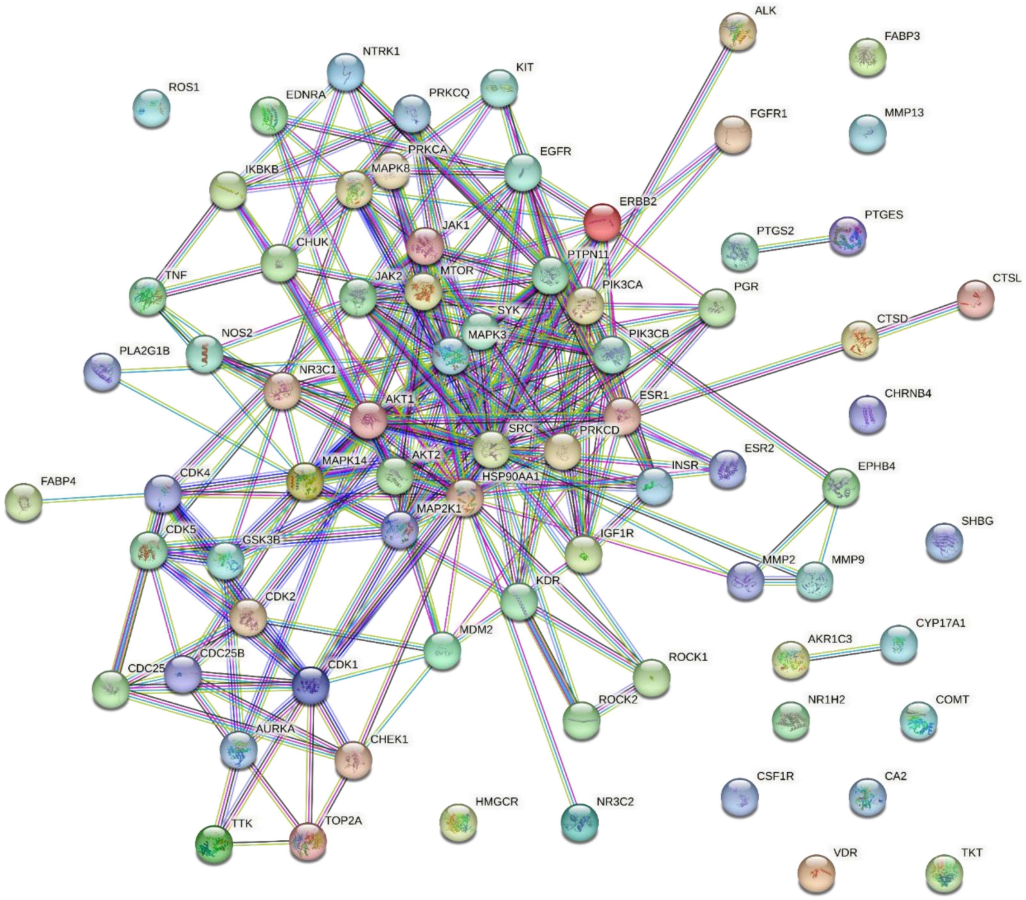

Figure 4.3. STRING protein-protein interaction of 74 target genes.

With a confidence level of 0.9, 12 target genes, namely NR1H2, MMP13, CHRNB4, CA2, CSF1R, HMGCR, COMT, ROS1, FABP3, SHBG, TKT & VDR were omitted, owing to zero-degree node interaction. On account of non-connectivity with a central hub, four target genes (PTGES, PTGS2, CYP17A1, and AKR1C3) with one-degree node connection, their average short path length, and closeness centrality as one were further excluded from the study. The protein-protein interaction of the resultant 58 target genes is shown in Figure 4.4.

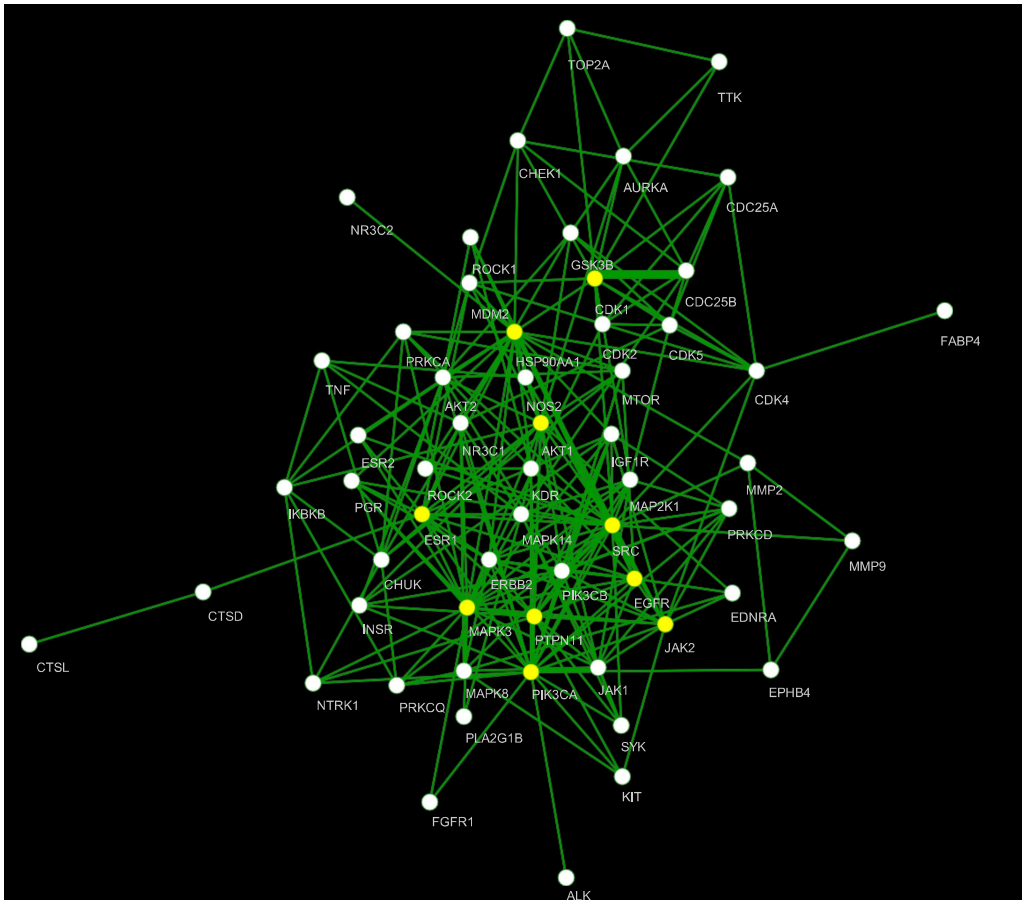

Figure 4.4. Protein-Protein interaction of 58 target genes. Yellow nodes represent the top 10 nodes based on degree.

The topological analysis consisting of degree, closeness centrality, and betweenness centrality of target genes are featured in Table 4.5.

Table 4.5. Topological analysis of protein-protein interaction of 58 target genes.

Target genes	Degree	Betweenness Centrality	Closeness Centrality
SRC	28	0.17968	0.655172
HSP90AA1	25	0.177424	0.626374
PIK3CA	25	0.131641	0.575758
MAPK3	22	0.09683	0.581633
AKT1	19	0.09388	0.581633
PTPN11	16	0.024138	0.53271
JAK2	15	0.035495	0.537736
ESR1	15	0.082991	0.553398
EGFR	13	0.013932	0.513514
CDK1	13	0.077057	0.504425

Table 4.5. Continued

Target genes	Degree	Betweenness Centrality	Closeness Centrality
MAPK14	12	0.041077	0.518182
PIK3CB	12	0.008383	0.491379
ERBB2	11	0.006067	0.5
JAK1	11	0.006631	0.491379
MAP2K1	10	0.021219	0.508929
IGF1R	10	0.007929	0.487179
CDK4	9	0.05634	0.495652
CHUK	9	0.010129	0.456
NR3C1	9	0.02757	0.518182
AKT2	9	0.010709	0.491379
MTOR	8	0.003482	0.478992
PRKCD	8	0.001443	0.471074
MAPK8	8	0.008967	0.463415
CDK5	8	0.009089	0.422222
MDM2	8	0.015103	0.478992
CDC25B	7	0.008068	0.395833
IKBKB	7	0.006397	0.448819
PRKCA	7	0.003077	0.467213
KDR	7	0.006357	0.478992
CDK2	7	0.010799	0.431818
PGR	6	7.21E-04	0.478992
AURKA	6	0.017177	0.419118
CHEK1	6	0.011838	0.431818
SYK	6	0.001523	0.456
INSR	6	7.26E-04	0.428571
CDC25A	6	0.001257	0.375
PRKCQ	6	0.005356	0.467213
GSK3B	6	0.007737	0.428571
TNF	5	0.003327	0.395833
NTRK1	5	0.003718	0.425373
NOS2	5	0.005183	0.459677
ROCK2	4	0	0.431818
MMP2	4	0.007101	0.435115
EDNRA	4	9.12E-04	0.413043
ROCK1	4	0	0.431818
ESR2	4	0	0.456
TOP2A	4	5.67E-04	0.351852
KIT	4	6.44E-04	0.407143
EPHB4	3	0.00263	0.385135
TTK	3	0	0.349693
MMP9	3	0.0018	0.407143
FGFR1	2	2.63E-04	0.407143
CTSD	2	0.035088	0.363057

Table 4.5. Continued

Target genes	Degree	Betweenness Centrality	Closeness Centrality
PLA2G1B	2	0	0.38255
FABP4	1	0	0.333333
NR3C2	1	0	0.387755
CTSL	1	0	0.267606
ALK	1	0	0.367742

The yellow-filled cells are the top 10 target genes.

The top 10 target genes based on topological analysis were SRC, HSP90AA1, PIK3CA, MAPK3, AKT1, PTPN11, JAK2, ESR1, EGFR, and CDK1 (indicated with yellow nodes in Figure 4.4). With the considerably high value of the degree, closeness centrality, and betweenness centrality, these target genes can be considered as nodes with high interaction, hub nodes, and nodes with potential control, respectively.

4.4.1.5. Gene enrichment analysis

The Shiny GO operating interface for GO enrichment was set at p-value ≤0.05, *i.e.*, based on false discovery rate (FDR), for analyzing target genes in three arenas: GO biological, GO cellular, and GO molecular. FDR represents how likely the enrichment is by chance. The obtained top 10 GO biological, GO cellular and GO molecular processes encompassing target genes are shown in Figure 4.5 (a-c). Similar operating settings were used for the KEGG pathway in the Shiny GO webserver. The top 10 enriched pathways involving target genes are represented in a dot plot, as shown in Figure 4.6. Out of 58 target genes, 33 target genes were involved in KEGG pathways of cancer, as shown in Figure 4.7. These 33 genes were majorly related to ESR1, EGFR, and its other RTK family member, the RAS-RAF-MEK pathway, PI3K-AKT-mTOR pathway, JAK-STAT pathway, and CDK.

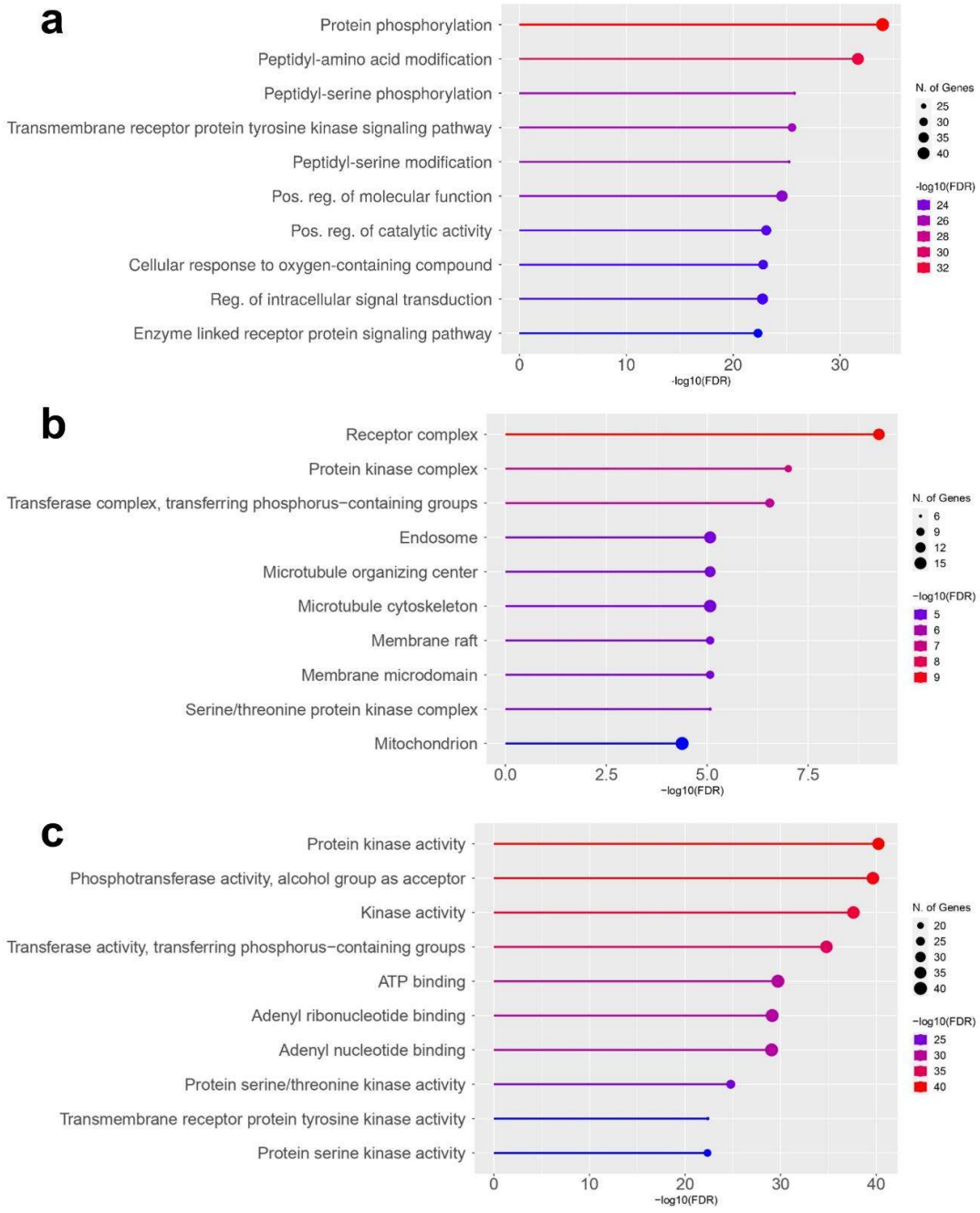

Figure 4.5. Top 10 Gene ontology enrichment in three arenas (a) biological process (b) cellular component, and (c) molecular function of 58 target genes.

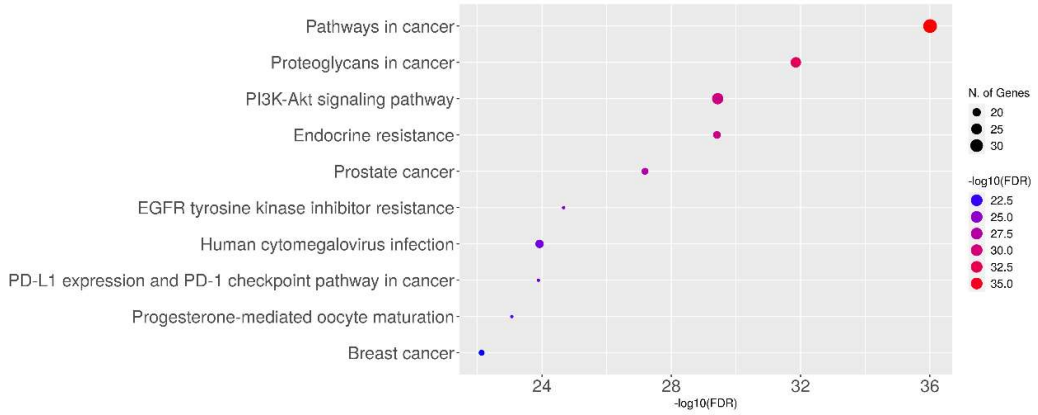

Figure 4.6. Dot plot of top 10 KEGG pathways of 58 target genes.

4.4.1.6. Network layout of compound-target

The Compound-target network of HFPO1 is shown in Figure 4.8. Owing to a lack of interaction with enriched 58 target genes, BET and MYX compounds were excluded from the network construction. The obtained network consists of 67 nodes (1 HFPO1 node, 8 myco-metabolites nodes, and 58 target genes nodes) interconnected by 108 edges (interaction). Based on degree, which indicates the number of interactions of particular nodes, the metabolites were ranked. MOM stands out with 33 degrees, followed by LAB with 21, LIN with 14, AST, and OPH with 13.

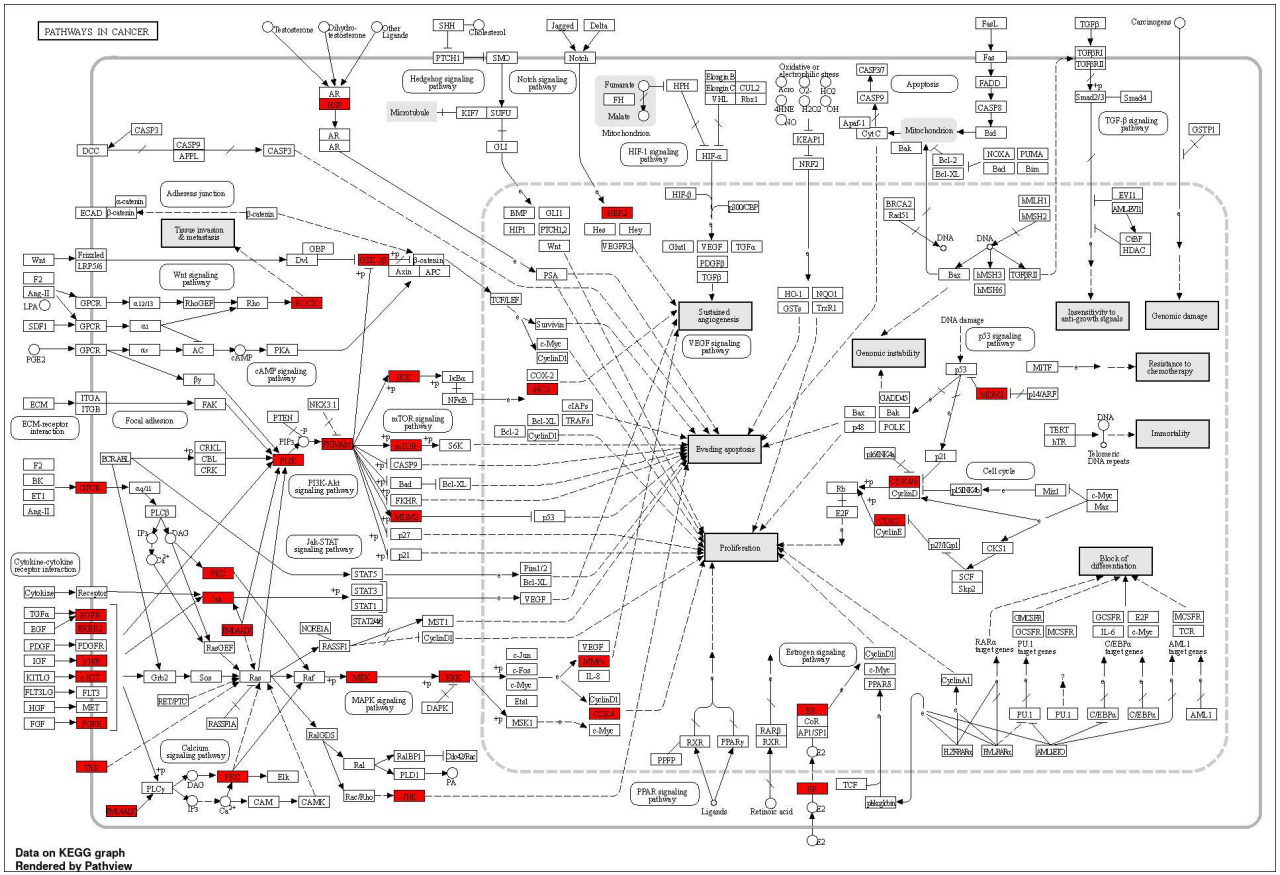

Figure 4.7. Target genes involved in KEGG's pathway of cancer.

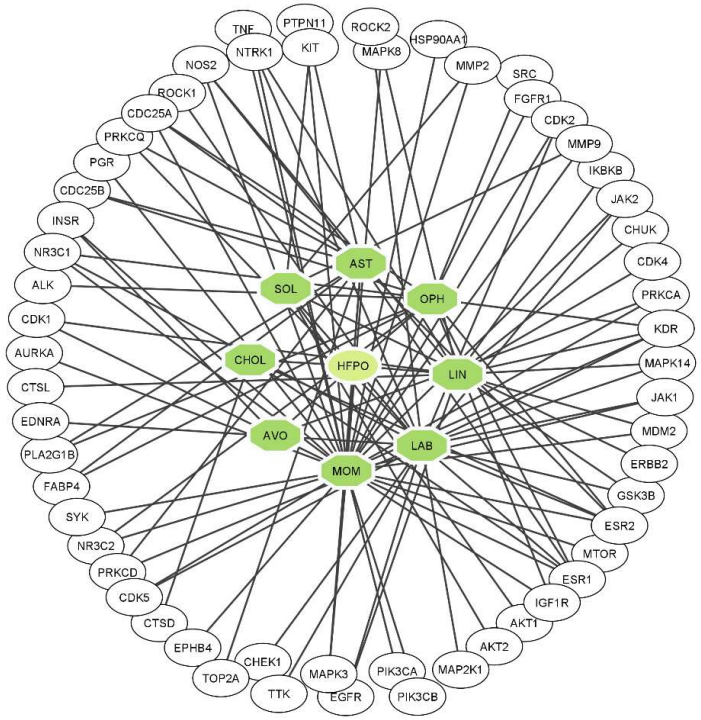

Figure 4.8. Interaction between myco-metabolites of HFPO1 with 58 target genes and top 10 KEGG pathways.

4.4.1.7. *In-silico* docking interaction of hub targets and key myco-metabolites

After analyzing protein-protein interaction and enrichment analysis of target genes, some of the influential hub target genes involved in the KEGG pathway of cancer were selected for studying structure-based design. The dock results of hub target genes EGFR (PDB Id: 6LUD), ESR1 (PDB Id: 6W0K), JAK2 (PDB Id: 6VGL), MAPK3 (PDB Id: 7M0Y), PIK3CA (PDB Id: 4JPS) and AKT1 (PDB Id: 4EKL) with their respective HFPO1 myco-metabolites is tabulated in Table 4.6. and pictorially demonstrated in Figure 4.9.

Table 4.6. Docking scores of hub target genes with their respective HFPO1 myco-metabolites.

	EGFR (PDB Id: 6LUD)	**ESR1 (PDB Id: 6W0K)**	**JAK2 (PDB Id: 6VGL)**	**MAPK3 (PDB Id: 7M0Y)**	**CDK1 (PDB Id: 6GU6)**	**PIK3CA (PDB Id: 4JPS)**	**AKT1 (PDB Id: 4EKL)**
LIN	**-7.24**				**-7.7**		
LAB	-6.04	-5.9	-6.6				
MOM		**-7.8**	**-8.8**	**-8.88**	-7.4	**-7.5**	
AST		-4.2		-6.59			
OPH		-4.14					
SOL							**-6.39**

Bold signifies the maximum score among each class of target genes.

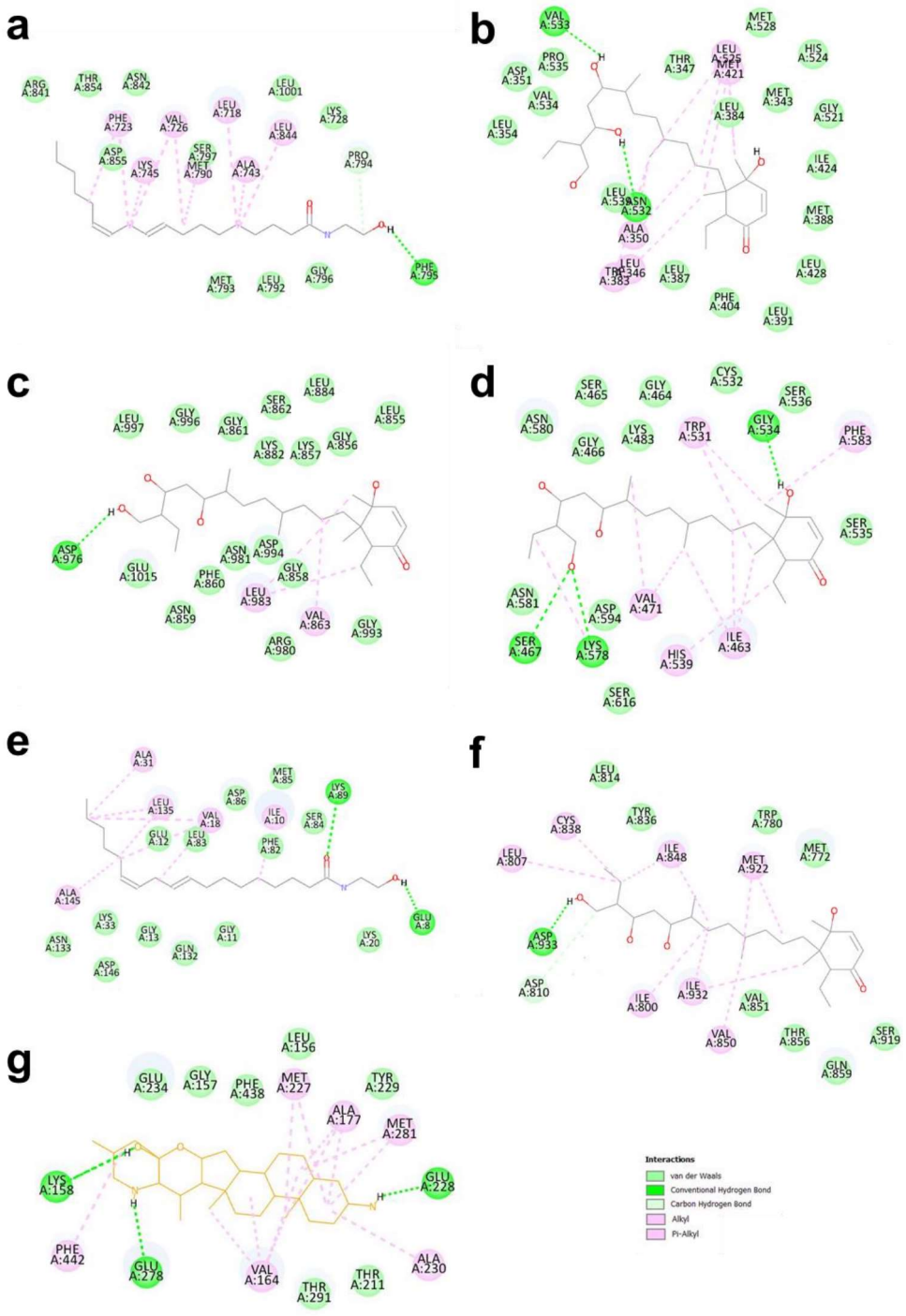

Figure 4.9. Molecular docking analysis of HFPO1 myco-metabolites with their respective target gene (a) LIN and EGFR (PDB Id: 6LUD) (b) MOM and ESR1 (PDB Id: 6W0K) (c) MOM and JAK2 (PDB Id: 6VGL) (d) MOM and MAPK3 (PDB Id: 7M0Y) (e) LIN and CDK1 (PDB Id: 6GU6) (f) MOM and PIK3CA (PDB Id: 4JPS) (g) SOL and AKT1 (PDB Id: 4EKL).

4.4.1.8. *In-silico* cancer multi-omics expression study & prognostic potential

GEPIA webserver was used for transcriptional expression study of hub genes among tumor and normal samples. The selected hub target PI3KCA, and ATK1 were highly expressed in acute myeloid leukemia samples as compared to normal tissue ($p < 0.05$) (Figure 4.10.a). For exploring the prognostic potential of PI3KCA, and ATK1 hub target for acute myeloid leukaemia, UALCAN webserver was used to analyse relationship of mRNA expression of the hub target with the overall survival (OS). As shown in Figure 4.10.b, low mRNA levels of PI3KCA, and ATK1 showed a good prognosis in breast cancer. However, the proteomic expression data of PI3KCA, and ATK1 for acute myeloid leukemia were unavailable.

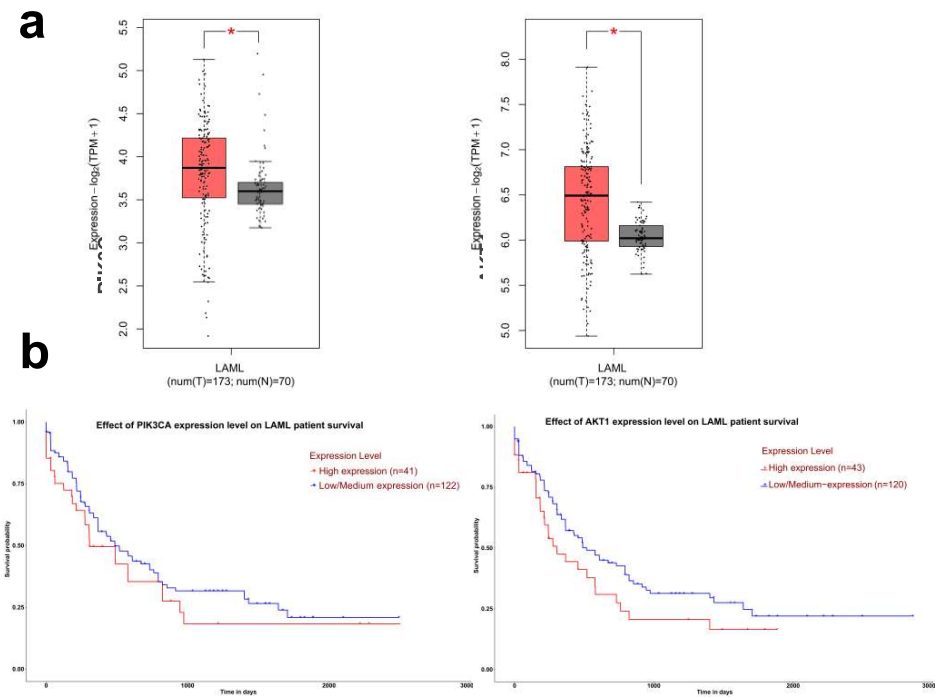

Figure 4.10. *In-silico* cancer multi-omic expression study and prognostic potential of selected hub target (PI3KCA, and ATK1) for acute myeloid leukaemia (a) genomic expression, and (b) overall survival analysis.

4.4.2. *In-vitro* experimental validation

4.4.2.1. Fluorescence microscopy

Morphological alterations at a nuclear level were visually inspected by fluorescence microscopy using nuclear staining dye DAPI. DAPI stained fluorescent photo micrograph clearly demonstrates (Figure 4.11.) a dose-dependent blebbing, nuclear fragmentation, and chromatin condensation of the treated cell, thus indicating induction of apoptosis.

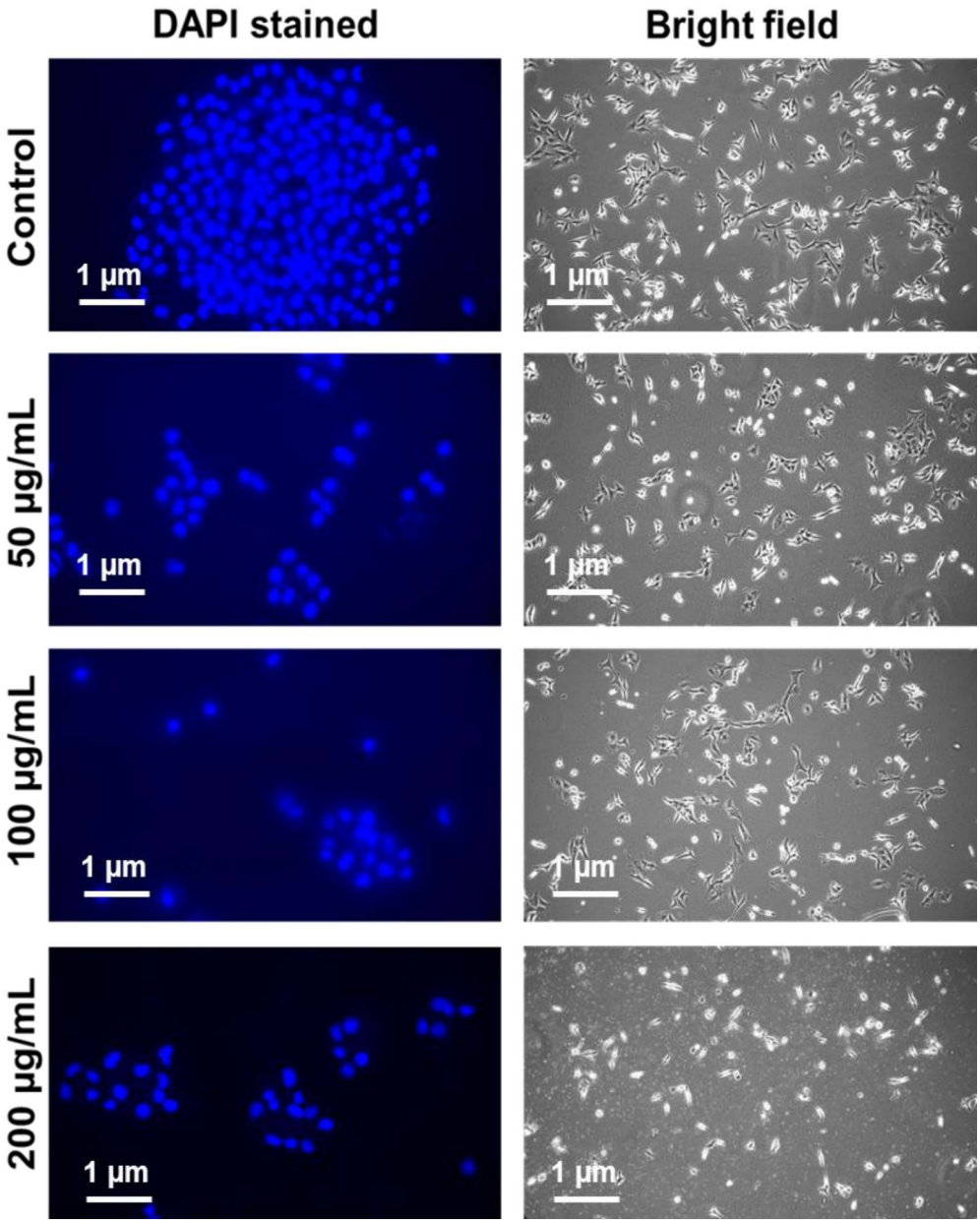

Figure 4.11. Fluorescence micrographs (DAPI stained) of untreated and treated HL-60 cancer cell line with HFPO1 (0-200 µg/mL). Scale bar: 1µm; Magnification: 20X.

4.4.2.2. Immunoblot analysis

Out of 56 target genes, 33 genes were linked to 'pathway in cancer' by KEGG pathway analysis. These 33 genes were majorly related to ESR1, EGFR, and its other RTK family member, RAS-RAF-MEK, PI3K-AKT-mTOR, JAK-STAT, and CDK. Whereas, from PPI interaction by STRING webserver, SRC, HSP90AA1, PIK3CA, MAPK3, AKT1, PTPN11, JAK2, ESR1, EGFR, and CDK1 were the hub target protein. Hence, to verify the reliability of obtained targets in network pharmacology, we have conducted immunoblot analysis for PI3KCA, AKT1, and mTOR protein to trace the signalling pathway involved in the anti-cancer potential of HFPO1. There was a dose-dependent decrease in p110α, AKT-473, and mTOR expression, as evident in Figure 4.12. Concluding, HFPO1 anticancer potential is due to the suppression of the PI3K-AKT-mTOR signalling pathway.

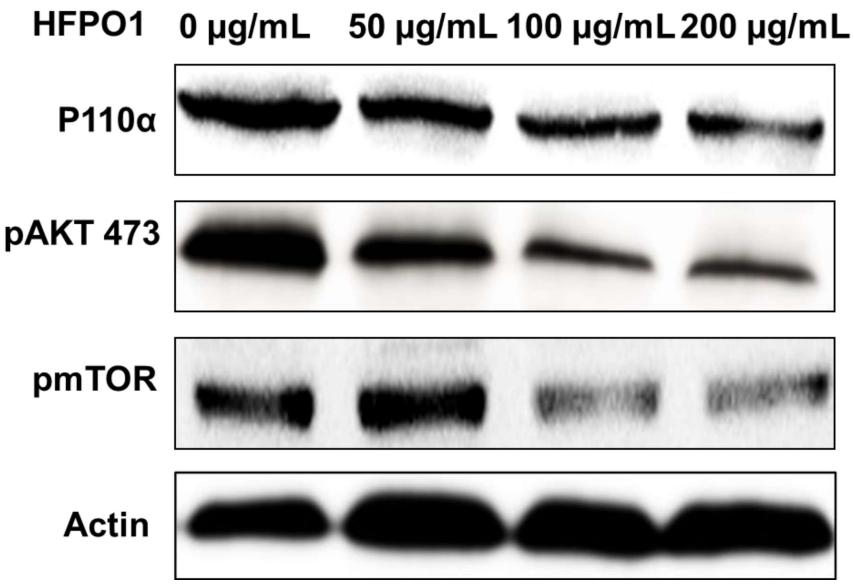

Figure 4.12. Immunoblot analysis using antibodies against P110α, AKT, and mTOR protein in HFPO1 treated HL-60 (0-200 µg/mL).

4.4.3. *In-vivo* experimentation

4.4.3.1. Acute toxicity assessment

The acute toxicity of HFPO1 was studied according to OECD 425 guidelines. At the doses 550 mg/kg and 2000 mg/kg, mortality was observed in Swiss albino mice. The remaining mice surviving 175 mg/kg were further observed for 14 days, and on the 15th day, they were humanely killed, and blood was collected for hematological and biochemical analysis. The biochemical and hematological parameters of surviving mice showed a non-significant difference from control mice ($p < 0.05$), as shown in Table 4.7. and Table 4.8., respectively. The difference in weight of mice on the 0th and 14th day was non-significant (Table 4.9.). No difference in histology architecture was seen in the liver and kidney of 175 mg/kg HFPO1 with respect to control mice, as reflected in Figure 4.13. The estimated LD_{50} determined from AOT425statpgm software was 301 mg/kg in Swiss albino mice, attached in *Appendix* (Figure A6).

Table 4.7. Biochemical parameters of HFPO1 (175 mg/kg) group against control Swiss albino mice for acute toxicity assessment.

Biochemical parameters	Control group	HFPO1 (175 mg/kg)
Glucose (mg/dL)	85.378 ± 5.891	80.075 ± 6.396
SGPT (U/L)	45.694 ± 4.201	46.600 ± 5.633
SGOT(U/L)	137.340 ± 6.284	142.975 ± 5.320
ALP(U/L)	40.759 ± 2.641	43.561 ± 1.741
Total protein (g/dL)	4.932 ± 0.998	5.251 ± 0.463
Urea (mg/dL)	48.520± 4.893	45.65 ± 3.517
Creatinine (mg/dL)	0.354 ± 0.027	0.450 ± 0.032
Triglyceride(mg/dL)	107.998 ± 7.095	113.817 ± 6.343
Cholesterol (mg/dL)	82.903 ± 4.357	77.376 ± 8.947

Values are expressed as Mean ± SD (n = 3). One-way ANOVA was performed followed by the turkey's multiple comparison test ($p < 0.05$), using Graph pad prism 5.0.

Table 4.8. Hematological parameters of HFPO1 (175 mg/kg) group against control Swiss albino mice group for acute toxicity assessment.

Hematological parameters	Control group	HFPO1 (175 mg/kg) group
Hemoglobin	10.238±3.872	9.899±1.045
WBC (White blood cell) (*10^3/µl)	8.805±1.786	9.243±1.254
RBC (Red blood cell) (*10^6/µl)	5.978±3.296	5.147±4.093
Packed Cell Volume (HCT) (%)	38.300±5.735	40.450±4.610
Mean Corpuscular Volume (MCV) (fL)	50.745±5.183	45.292±3.392
Mean Corpuscular Hemoglobin (MCH) (pg)	29.045±4.793	31.983±3.715
Mean Corpuscular Hemoglobin Conc. (%)	32.931±2.692	35.342±1.836
RDW (%)	16.804±2.539	14.261±2.493
Platelets Count (*10^5/µl)	7.897±3.814	6.325±4.934

Values are expressed as Mean ± SD (n = 3). One-way ANOVA was performed followed by the turkey's multiple comparison test ($p < 0.05$), using Graph pad prism 5.0.

Table 4.9 Change in weight (g) of HFPO1 (175 mg/kg) group in Swiss albino mice for acute toxicity assessment.

	0^{th} day	14^{th} day
Body weight (g)	24.524 ± 0.575	25.137 ± 0.849

Values are expressed as Mean ± SD (n = 3). One-way ANOVA was performed followed by the turkey's multiple comparison test ($p < 0.05$), using Graph pad prism 5.0.

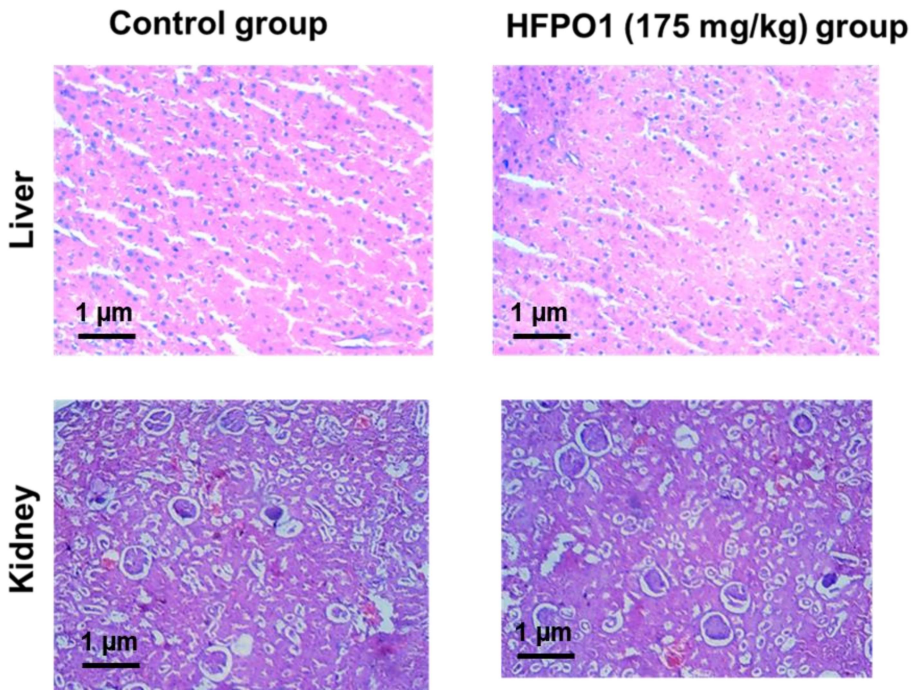

Figure 4.13. Histopathological examination of liver and kidney of HFPO1 (175 mg/kg) group against control Swiss albino mice group for acute toxicity assessment. Scale bar: 1µm; Magnification: 10X.

4.4.3.2. *In-vivo* anti-tumor efficacy in EAC (solid tumor) bearing Swiss albino mice

A reduction in tumor size, tumor volume, and tumor weight of EAC (solid tumor) bearing Swiss albino mice are indicative of *in-vivo* therapeutic efficacy. As compared to tumor-bearing mice 'T' with tumor volume (980.4072 ± 53.2112 mm^3), the tumor volume of treated groups H1, H2, H3, and S were measured at approximately 427.012 ± 32.0758 mm^3, 381.3405 ± 40.4159 mm^3, 300.7014 ± 39.4502 $mm^3$and 83.755 ± 38.0269 mm^3 respectively, thus indicating a significant difference ($p < 0.05$) (Figure 4.14.a). Similarly, there was a significant reduction in tumor weight in the treated groups H1, H2, H3, and S (Figure 4.14.b), in contrast to tumor-bearing mice 'T'. The average tumor growth inhibition index of the treated groups H1, H2, H3, and S was found to be 56.45%, 61.1%, 69.3%, and 91.46%, respectively, as reflected in Figure 4.14.c. The reduction in tumor volume of the treated group as compared to the untreated group is pictorially represented in Figure 4.14.d. Amongst the treated group, a significantly higher reduction in tumor volume and tumor weight was observed with S group, followed by H2, and H3 ($p < 0.05$). Biochemical parameters (glucose, SGPT, SGOT, ALP, Urea, Creatinine, Cholesterol, and total triglycerides) were in accordance with the control mice, thus indicating non-toxicity as shown in Table 4.10. Contrarily, a significant difference was observed in the biochemical parameters (glucose, SGPT, SGOT, ALP, urea, cholesterol, and triglycerides) of tumor-bearing mice as compared to the treated and control group. Further, non-significant differences in the weight of control, tumor-bearing mice, and treated mice on the 0^{th} day and 15^{th} day were observed, as reflected in Table 4.11. No mortality was observed during treatment. With the presented result, HFPO1 can be

identified as safe and efficacious in anti-tumor activity, in a dose of 10 mg/kg and 15 mg/kg against EAC (solid tumor) bearing Swiss albino mice.

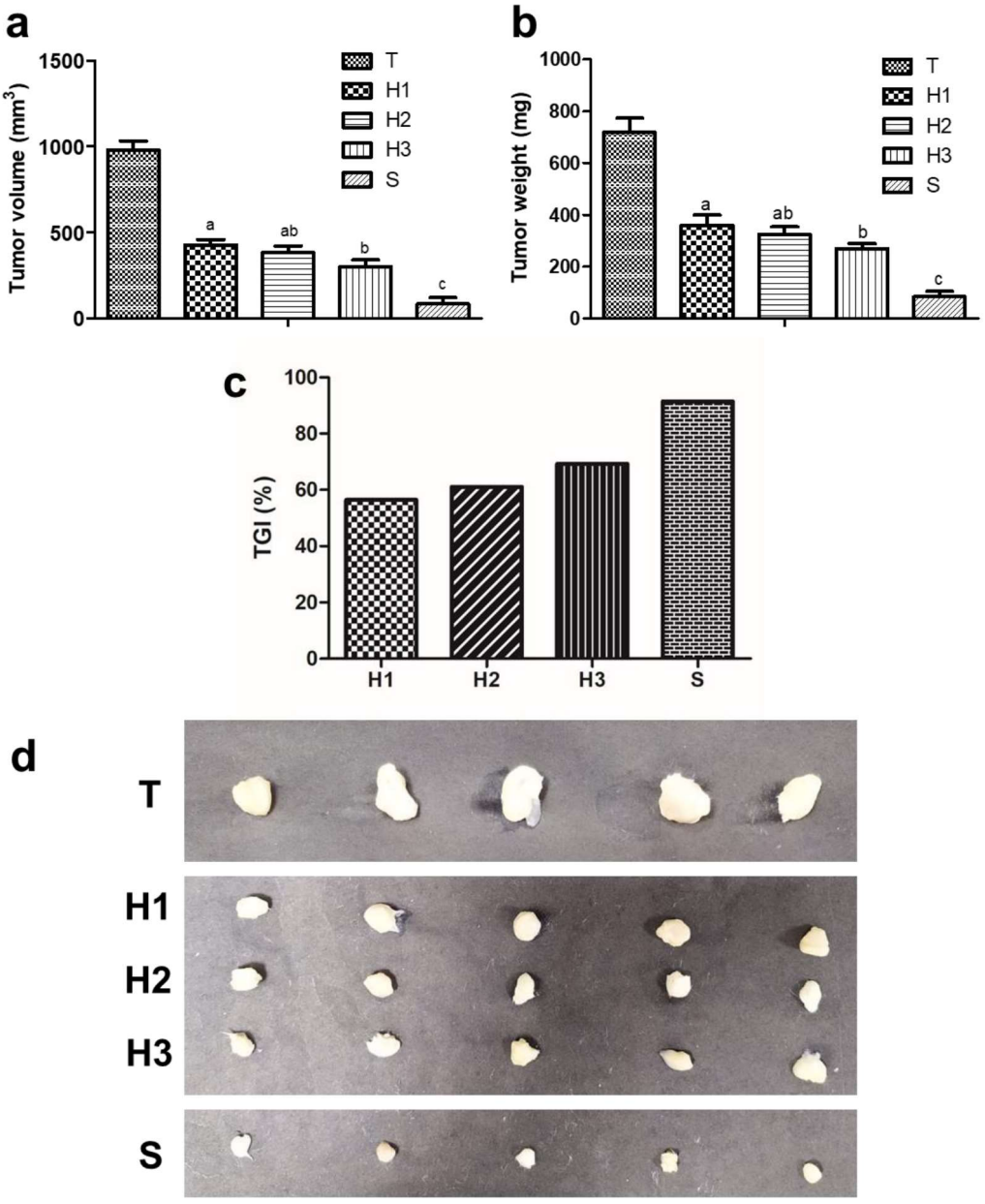

Figure 4.14. *In-vivo* anti-tumor efficacy in EAC (solid tumor) bearing Swiss albino mice. Values are expressed as Mean ± SD (n = 5). One-way ANOVA was performed, followed by the turkey's multiple comparison test ($p < 0.05$), using Graph pad prism 5.0. Different letters (a, b, and c) represent a significant difference at $p < 0.05$ & same letters represent absence of significant difference.

Table 4.10. Biochemical parameters of control group, tumor-bearing mice group (T), and treated group (H1, H2, H3, and S) of tumor-bearing mice.

Biochemical parameters	Control	T	H1	H2	H3	S
Glucose (mg/dL)	83.9 ± 2.885	135.249 ± 5.369***	86.42 ± 3.194	88.928 ± 5.705	89.682 ± 3.103	80.64 ±4.741
SGPT (U/L)	46.066 ± 3.489	60.237 ± 6.12*	49.258 ± 8.078	48.296 ± 5.295	40.966 ± 6.189	36.97 ±4.619
SGOT(U/L)	137.038 ± 6.564	168.919 ± 4.903***	145.572 ± 4.574	142.002 ± 7.964	143.546 ± 5.287	148.334 ±8.927
ALP(U/L)	39.4428 ± 5.520	68.603 ± 6.351***	47.354 ± 3.215	49.222 ± 2.873	45.77 ± 4.093	44.78 ±5.073
Urea (mg/dL)	48.667 ± 6.707	72.006 ± 3.854***	51.258 ± 6.326	54.296 ± 3.024	47.566 ± 6.612	46.37 ±3.675
Creatinine (mg/dL)	0.412 ± 0.067	1.724 ± 0.0789	0.358 ± 0.094	0.378 ± 0.111	0.396 ± 0.055	0.416 ±0.064
Triglyceride(mg/dL)	113.038 ± 6.916	140.365 ± 5.987***	119.772 ± 4.512	110.002 ± 6.632	117.546 ± 6.855	118.334 ±4.493
Cholesterol (mg/dL)	78.7 ± 3.767	108.654 ± 4.247***	82.42 ± 5.417	86.928 ± 6.726	84.682 ± 3.360	88.64 ±3.997

Values are expressed as Mean ± SD (n = 5). One-way ANOVA was performed, followed by the turkey's multiple comparison test ($p < 0.05$), using Graph pad prism 5.0. *** represent a significant difference at $p<0.05$ & * represent a significant difference at ($p < 0.01$).

Table 4.11. Change in weight (g) of the control group, tumor-bearing mice group (T), and treated group (H1, H2, H3, and S) of tumor-bearing mice.

Groups	Body weight (g)	
	0th day	**15th day**
Control	25.426 ± 3.983	27.170 ± 1.320
T	25.521 ± 3.732	26.376 ± 3.241
H1	25.902±2.391	26.783±1.567
H2	24.897±2.919	25.505±2.258
H3	25.425±1.664	27.199±3.754
S	24.383±3.250	25.263±2.861

Values are expressed as Mean ± SD (n = 5). One-way ANOVA was performed followed by the turkey's multiple comparison test ($p < 0.05$), using Graph pad prism 5.0.

4.5. Summary

Acquired drug resistance is observed with untargeted as well as targeted chemotherapies, although mechanisms differ. Compensatory and redundant molecular signalling, over-expression of target protein, inhibition of DNA repair mechanisms, target mutation acquired during treatment, activation of pro-survival signalling, inactivation of pro-apoptotic pathways, upregulation of tumor cell efflux transporters and epithelial-mesenchymal transition contribute to acquired drug resistance. For drug resistance acquired, owing to mutation or activation of complementary or redundant molecular pathways, a rational combinatorial target approach is a promising solution (Yip & Papa, 2021).

The overlapping target genes of myco-metabolites-target and disease-target are displayed in Figure 4.2. These are the influential targets genes of myco-metabolites of HFPO1, for cancer disease. For the treatment and management of breast and prostate cancer, endocrine therapy/hormonal therapies are used. Because of the high prevalence of ER-positive BC, treatments that inhibit the hormone's tumorigenic function are constantly being developed. Selective estrogen receptor modulators, selective estrogen receptor degraders, and aromatase inhibitors are some of the therapy options for inhibiting estrogen function (C. X. Ma et al., 2015)(Wardell et al., 2011). Through network analysis of PPI interaction (Figure 4.4.), ESR1 (Estrogen receptor 1) was identified as one of the hub target genes with a high number of interactions. Compounds MOM, LAB, AST, OPH, CHOL, and AST targets ESR1 target protein (Figure 4.8.). Despite positive outcomes and increased survival rates to treatments, resistance to such hormonal therapies develops. This estrogen receptor can cross-talk with various receptor tyrosine kinases (RTKs) like EGFR, FGFR, and HER (Borg et al., 1994)(Newby et al., 1997).

Hence, molecular signalling through the participation of redundant or alternative RTKs such as EGFR, FGFR, and HER can lead to the reactivation of ER- regulated transcription programs and tumor cell growth.

RTKs are responsible for growth-promoting signals. Under physiological settings, RTK activation begins with the binding of growth factors and hormones, followed by oligomerization and trans autophosphorylation, and finally, the initiation of downstream signalling cascades via complex substrate protein phosphorylation. Cell proliferation, differentiation, and survival are all regulated by these downstream signalling pathways, which include PI3K/AKT, Ras/MEK/ERK, PLC/PKC, and JAK/STAT. Moreover, they also upregulate the expression of genes responsible for epithelial-mesenchymal transition, an important step in cancer cell migration and invasion, involved in metastasis (Yip & Papa, 2021). They can be found in the mutant, amplified, and constitutively active states in cancer, thereby constantly transducing growth signals even when upstream stimuli are not present. Monoclonal antibodies and specific inhibitors are being used to combat this. Based on a topological feature assessment of protein-protein interaction target genes, EGFR (a member of the RTKs family), was identified as one of the hub target genes (Figure 4.4.) and a probable target for LIN and LAB compounds (Figure 4.8.). Resistance to EGFR-targeted therapy can still be developed due to the activation of other complementary RTKs members and downstream PI3K-AKT and Ras-MEK-ERK pathways (Luo & Fu, 2014)(Ludovini et al., 2011). In the presented studies, there were other members of the RTKs family, such as ERBB2, IGFR, FGFR, and c-KIT, identified as target genes for the tentative compound identified (Figure 4.7.).

The PIK3K/AKT pathway, a well-known downstream RTK signalling pathway, is involved in cell proliferation, differentiation, and survival. External stimuli such as growth factors, cytokines, and hormones are known to activate PI3K. PI3K catalyzes the

conversion of PIP2 (phosphatidylinositol-4,5-biphosphate) to the secondary messenger PIP3 (phosphatidylinositol-3,4,5 triphosphate) after activation. PIP3 bind and recruits several lipid-binding domains of downstream targets like PDK1 and MTORC2, which catalyze AKT1 phosphorylation. Phosphatase and tensin homologue deleted on chromosome 10 (PTEN) controls the pathway by dephosphorylating PIP3 to PIP2, which inhibits downstream kinases (Yip & Papa, 2021). The PI3K signalling pathway is frequently activated in tumors that are resistant to endocrine and RTK- targeted therapies. In the current study, PI3KCA was illustrated as one of the prominent target proteins with maximum interaction in protein-protein networking (Figure 4.4); this protein was a probable target for MOM compound (Figure 4.8.).

The proto-oncogene AKT is responsible for mTOR activation and has three isoforms (AKT1, AKT2, and AKT3). Constitutive activation of AKT, owing to a mutation in upstream RTKs, PI3K, and PTEN, has been involved in various cancer types. Thus, the upregulation of AKT activation has been associated with resistance to chemotherapies, making it a potential target for treatment (Yip & Papa, 2021). In the current framework of protein-protein interaction, AKT1, notified as one of the prime target proteins with the highest number of edges (Figure 4.4), was a target for SOL (Figure 4.8.).

RTKs activation promotes the activation of Ras protein, Ras activation recruits, and activates downstream targets Raf, active Raf phosphorylates, and activates MEK and ERK kinases, resulting in ERK 1/2 nuclear translocation, promoting cell proliferation and differentiation (Yip & Papa, 2021). In the current study, MOM myco-metabolite targets MAPK3 (Figure 4.8.), one of the potential hub targets identified in protein-protein interaction (Figure 4.8.).

Over and above this, HFPO1 myco-metabolites also targets JAK/STAT pathway, CDK, and MDM2. Synergistically, besides targeting multiple key signalling pathways involved in cancer, HFPO1 myco-metabolites also targets compensatory and redundant pathway, thus overcoming drug resistance.

The top KEGG pathway (Figure 4.6. and Figure 4.7.) describes the importance of 33 target genes involved in the cancer pathogenesis, particularly ESR1, EGFR, and its other RTK family members, Ras/Raf/Mek pathway, PI3K/AKT/mTOR pathway, JAK/STAT, and CDK. Gene ontology's top biological process, cellular component, and molecular function were protein phosphorylation, receptor complex, and protein kinase activity, respectively. Altogether, the above-described gene ontology was related to the RTK family member (Figure 4.5.), a key player involved in the KEGG pathway of cancer, modulating multiple downstream signalling pathways like Ras/Raf/Mek pathway, PI3K/AKT/mTOR pathway, and JAK/STAT.

In addition to this, the docking study further validates target prediction. Hub targets showed a good binding affinity with their respective HFPO1 myco-metabolites (Figure 4.9.). On the basis of the results obtained from network pharmacology, cell-viability assay, immunoblot analysis of PI3K/AKT/mTOR, fluorescence microscopy, and anti-tumor activity against EAC (solid tumor) bearing Swiss albino mice were investigated. Results signify evidence of apoptotic bodies from fluorescence microscopy (Figure 4.11.), modulation of PI3K/AKT/mTOR signalling pathway (Figure 4.12.), and significant decrease in tumor volume and tumor weight of HFPO1 treated EAC bearing Swiss albino mice (Figure 4.14.).

Collectively, this study scientifically traces the anti-cancer mechanistic approach of HFPO1 through network pharmacology, *in-vitro* immunoblot analysis, and *in-vivo* anti-tumor activity.